Tomas Bata University in Zlín
Library

Monitoring of corrosion extent in steel S460MC by the use of magnetic Barkhausen noise emission

Citation

JANČULA, Miroslav, Miroslav NESLUŠAN, Filip PASTOREK, Martin PITOŇÁK, Vladimír PATA, Peter MINÁRIK, and Jozef GOCÁL. Monitoring of corrosion extent in steel S460MC by the use of magnetic Barkhausen noise emission. *Journal of Nondestructive Evaluation* [online]. vol. 40, iss. 3, Springer, 2021, [cit. 2023-05-16]. ISSN 0195-9298. Available at https://link.springer.com/article/10.1007/s10921-021-00803-8

DOI

https://doi.org/10.1007/s10921-021-00803-8

Permanent link

https://publikace.k.utb.cz/handle/10563/1010493

This document is the Accepted Manuscipt version of the article that can be shared via institutional repository.

TBU Publications
Repository of TBU Publications
publikace.k.utb.cz

Monitoring of Corrosion Extent in Steel S460MC by the Use of Magnetic Barkhausen Noise Emission

M. Jančula[1], M. Neslušan[2], F. Pastorek [3], M. Pitoňák[1], V. Pata[4, 5], P. Minárik[3,5]. J. Gocál[1]

[1]Faculty of Civil Engineering, University of Žilina, Univerzitná 1, 01026 Žilina, Slovakia Email: *miroslav.jancula@uniza.sk, Email: jozef.gocal@uniza.sk*

[2]Faculty of Mechanical Engineering, University of Žilina, Univerzitná 1, 01026 Žilina, Slovakia Email: *miroslav.neslusan@fstroj.uniza.sk*

[3]Research Centre, University of Žilina, Univerzitná 1, 01026 Žilina, Slovakia Email: *filip .pastorek@ uniza.sk*

[4]Faculty of Technology, Tomas Bata University in Zlín, Zlín, Czech Republic Email: *V.Pata pata@utb.cz*

[5]Faculty of Mathematics and Physics, Charles University, Ke Karlovu 5, 121 16 Praha 2, Czech Republic *Email: Peter.Minarik@mff.cuni.cz*

Abstract

Monitoring of corrosion extent is critical in bridge operation and civil buildings. Reducing the effective cross-sectional area of components can redistribute the stress state and increase the true stress in the critical parts of civil structures. Unexpected rupture of bodies can occur as a result of their over-stressing. However, it is not possible to take relevant samples from these structures for a laboratory analysis during their lifetime. For this reason, this study investigates the potential of magnetic Barkhausen noise analysis for real-time corrosion extent monitoring. This study demonstrates that Barkhausen noise emission drops down along with an increasing degree of corrosion of steel S460MC. Progressive and remarkable decrease of Barkhausen noise and alteration of extracted features result from increasing surface roughness and superimposing influence of the increasing thickness of the near-surface layers containing mainly iron oxides. Furthermore, it was found that corrosion on the surface also alters the relation between tensile stress and Barkhausen noise within the interaction volume.

Keywords: Magnetic Barkhausen noise, corrosion, tensile stress, non-destructive technique

1 Introduction

Magnetic Barkhausen noise (MBN) can be detected in ferromagnetic materials as a result of domains and especially domain walls (DWs) motion [**1-3**]. DWs encounter lattice perturbations whereupon their motion is not smooth by discontinuous generating acoustic as well as electromagnetic impulses detectable by suitable coils. Therefore, MBN signals contain information about the diverse lattice defects. Moreover, the strength and time distribution of MBN impulses are governed by the stress state [**4-8**] that affects the configuration of DWs with respect to the direction of exerted load. Prevailing of stress state or microstructure depends on the magnetic hardness and/or magnetostriction. Matrix defects are considered as pinning sites affecting the magnetic field necessary to unpin DWs. Furthermore, the density, morphology, and size of these perturbations (such as dislocations, carbides, grain boundaries, or non-ferromagnetic phases) affect the average distance for

the free DWs motion [**8-12**]. For these reasons, MBN is very often employed for monitoring of parts in which altering microstructure and/or stress are considered.

This technique has been already reported as a promising method for measurement of the real stress state in the highway bridge [**13**]. Furthermore, detection of wires over-stressing [**14**], their corrosion damage [**15**], and assessment of the real pre-stress in tendons [**16**] has been also discussed. Components in bridges or civil constructions are usually loaded in the elastic region of stresses. However, corrosion attack can decrease the effective cross-sectional area, which in turn increases true stress. True stress in heavily corroded bodies can exceed the yield strength of components. As soon as the plastic deformation becomes more developed, failure of constructions could be expected since the loss of bearing capacity accelerates the over-loading of structures in their important regions (load redistribution) [**17, 18**].

It has been already investigated that increasing the corroded layer's thickness on the surface attenuates the MBN signal and increases the surface's magnetic hardness [**15**]. However, such evolution saturates as soon as the corroded layer thickness exceeds 300 μm in the case of high-strength steel wires as the main bearing components of bridges. This topic is vital of importance but the papers directly dealing with this topic are really rare [**15, 19, 20**]. The pilot study in which the real bridge stress state was monitored via MBN technique was carried on the new bridge [**13**]. However, monitoring of real bridges with respect of their long term operation represents the task in which stress state and corrosion damage of variable extent are superimposed. Therefore, this study investigates influence of corrosion attack artificially developed in corrosion chamber as well as the influence of the corrosion extent on the relationship between MBN (variety of MBN features) and amplitude of tensile stress. The potential of the MBN technique to assess the corrosion extent of ferritic steel S460MC is discussed in chapter 3.1 whereas the influence of layer of the different thickness on the relation between the tensile stress and MBN parameters extracted from the raw MBN signals is reported in chapter 3.2.

2 Experimental Conditions

Experiments were carried out on the 60 (20 series of 3 samples) samples of dimensions 50 x 50 x 5 mm and 12 samples of dimensions 150 x 15 x 5 mm (employed for the tensile test) made of steel S460MC (yield strength 540 MPa, ultimate strength 610 MPa, for chemical composition please check **Table 1**). The microstructure of S460MC is composed of fine ferrite (appears white on optical images) and small pearlite area (appears dark on optical images), as **Fig. 1** depicts.

Table 1 Chemical composition of S460MC in wt%

Fe	C	Mn	Si	P	S	Al	Ti	Nb	V
Balance	0.082	1.040	0.019	0.006	0.003	0.055	0.001	0.050	0.054

The samples were subjected to the corrosion attack at the laboratory conditions. In order to accelerate the corrosion progress, a corrosion test was performed in a simulated neutral salt spray atmosphere according to STN EN ISO 9227 standard in Votsch VSC KWT 1000 corrosion chamber. The test was carried out at a constant temperature of 35 °C. The sodium chloride solution for salt spray production was prepared by dissolution of pure sodium chloride in deionized water (conductivity not higher than 20 μS/cm) with a concentration of 50 g/l ± 5 g/l at 25 °C. The pH of the solution was between the required range from 6.5 to 7.2 during the whole salt spray test. In order to prevent the evaporation of water from the sprayed droplets, the air was humidified before entering the atomizer by passage through a saturation tower containing water with a temperature of 45 °C. The absolute pressure of the used compressed air was set to 120 kPa. The samples were thoroughly cleaned prior to the test and subsequently attached to the corrosion chamber by inert plastic stripes. The samples were subjected to salt spray atmosphere for various exposure times from 1 to 65 days. In order to carry out the repetitive measurements, three samples were removed from the chamber on the same day. Loose corrosion residues were gently (manually) removed from the surface of each sample by a wire brush. Afterwards, the surface was water cleaned and dried. Some of the samples were prepared for metallographic observations: cold moulded in Epofix resin, ground, polished and etched by 3% Nital for 5 s. The samples' macro and microstructure were observed using the light microscopes Zeiss AxioCam MRc5 and Olympus SZx16. Evaluation of the effective (reduced) wall thickness and the thickness of corrosion products layer was carried out in Quick Photo Industrial 3.0 software (in five different positions). Additional investigation of the crosssections was performed with a scanning electron microscope (SEM) FEI Quanta FX200.

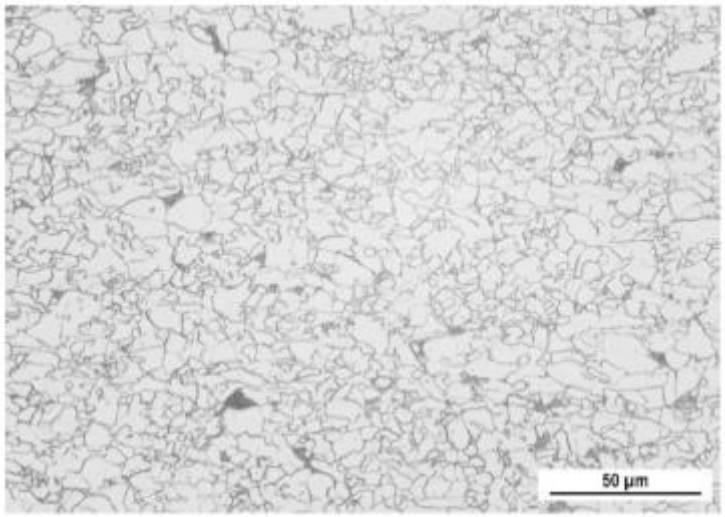

Fig. 1 Fine ferrite matrix of S460MC, 3% Nital

Specifications for MBN measurements are listed in **Table 2**. MBN signals were acquired from the unloaded surfaces as well as the samples loaded by tensile stresses (TS) below the matrix yielding by the use of Instron 5985 device. Load of bridges with respect of their long-term operation is mostly a combination of mechanical load and the superimposing corrosion damage. For this reason, MBN emission is investigated as a function of variable uniaxial tensile stress developed in the corroded samples as well.

Scanning of surface topography and evaluation of *S* (area extension of standard surface roughness R parameters measured in line) parameters (*Sa*—arithmetical mean height, *Sq*—root mean square height and *Sz*—maximum height) was carried out using 3D scanner Zygo Newview 8000. This system employs Coherence Scanning Interferometry, which combines Vertical Scanning Interferometry and Phase Shifting Interferometry (scanning speed 50 um s^{-1}, scanned height 1000 um, magnification of scanned area 12.5x, scanned area 3 × 3 mm).

3 Results of Experiments and Their Discussion

3.1 Unloaded Samples

Figure 2 illustrates the surface topography exposed to the aggressive corrosion attack. These figures demonstrate the strong non-homogeneity of surface topography in the neighbouring regions as a result of the specific character of the corrosion process. The adjacent regions of the surface become relatively anodic or cathodic to each other.

Table 2 Details about MBN measurements

Device	Roll scan 350
Software	Micro scan 600
Magnetising voltage	±5 V which correspond the magnetising field ±4.6 kA.m^{-1} (measured by Gauss meter)
Magnetizing frequency	125 Hz, sine profile
Frequency range of MBN pulses	50÷700 kHz
Number of MBN bursts	6
Estimated reading depth	about 0.5 mm (decreasing with more developed corrosion damage)
Sensor	Bipolar, S1-18-12-01
Sampling frequency	6.4 MHz
Direction of MBN measurement	EA (easy axis)—direction of sheet rolling HA (hard axis)—perpendicular to EA
MBN parameters	MBN—rms values of Barkhausen emission Number of MBN pulses *PP*—position of MBN envelope maximum *FWHM*—full width at half maximum of the MBN envelope

This potential can be reversed which expands corrosion attack into the adjacent non-corroded regions. The presence of chlorides accelerates the overall corrosion of the steel surface. From the thermodynamical point of view, the corrosion process preferentially attacks the weakest regions of the matrix. For this reason, the corrosion depth in some areas can remarkably vary, as **Fig. 2** depicts. It can be found that the depth and size of corrosion pits (holes or valleys which appear blue in **Fig. 2**) grew with time during exposure to the aggressive environment.

Figure 3 shows that surface roughness parameters such as Sa, Sq and Sz increase with the number of exposure days in the corrosion chamber. **Figure 4** illustrates that the long-term corrosion attack also reduces the wall thickness, which corresponds with the decrease of the samples' effective crosssectional area. Furthermore, **Fig. 5** depicts that the corroded layer, which thickness increases with the exposure time, covers the samples' surface.

Figure 6 presents quantification of this process and demonstrates that increasing thickness of the corroded layer on the surface is inversely proportional to the wall thickness obtained from **Fig. 4**.

Figure 7 presents SEM micrographs, which provide higher magnification of the corroded layer. It is visible that this corroded layer is composed of dark, grey and white regions. Analysis of the chemical composition of the individual areas corresponding to the different shades of grey has been reported in the previous study focused on corrosion of steel wires **[15]**. The local chemical analysis proved that the dark area can be linked to a/8-FeOOH and the grey one to Fe_3O_4 [**21, 22**], whereas the white regions represent the non-corroded steel fragments [**15**].

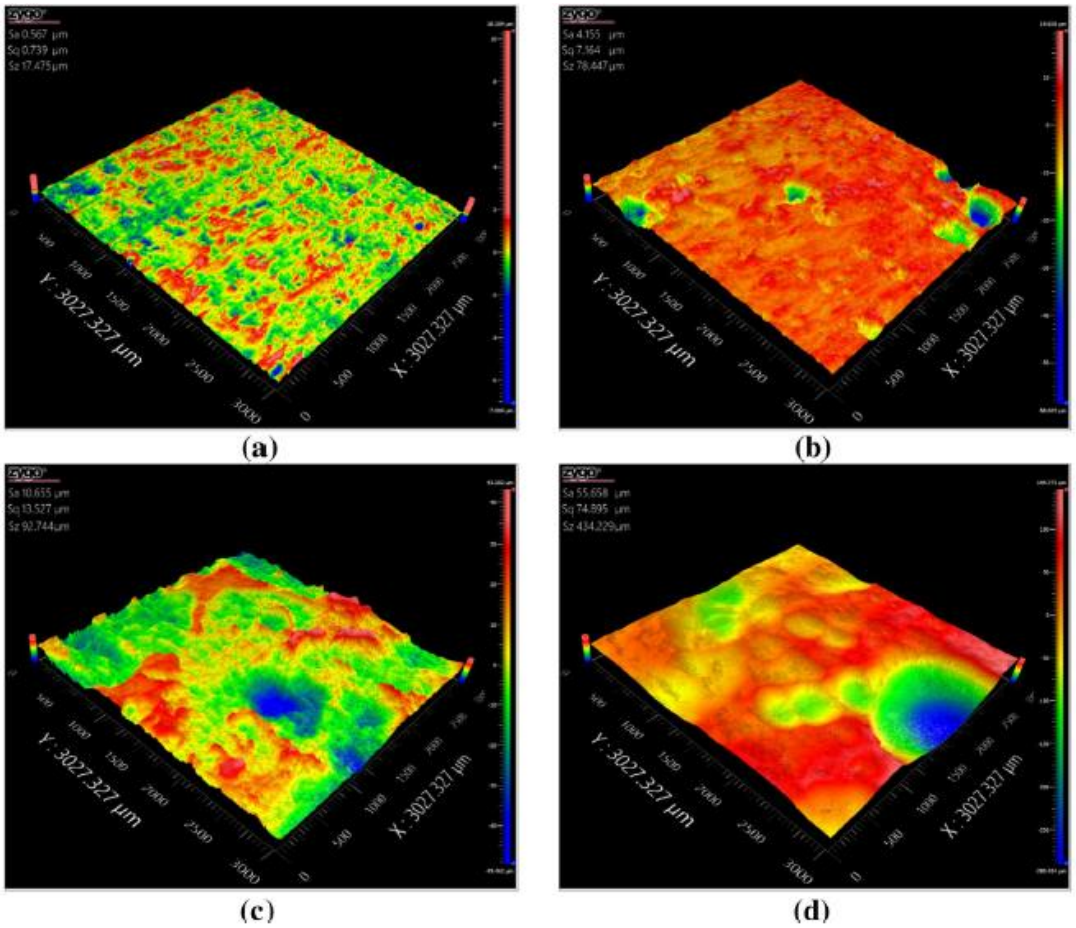

Fig. 2 Surface topography of corroded samples: **a** non-corroded bulk, color scale from — 7 to 10 µm, **b** 1 day in the chamber, color scale from — 58 to 20 µm, **c** 14 days in the chamber, color scale from — 50 to 43 µm, d 65 days in the chamber, color scale from — 290 to 145 µm

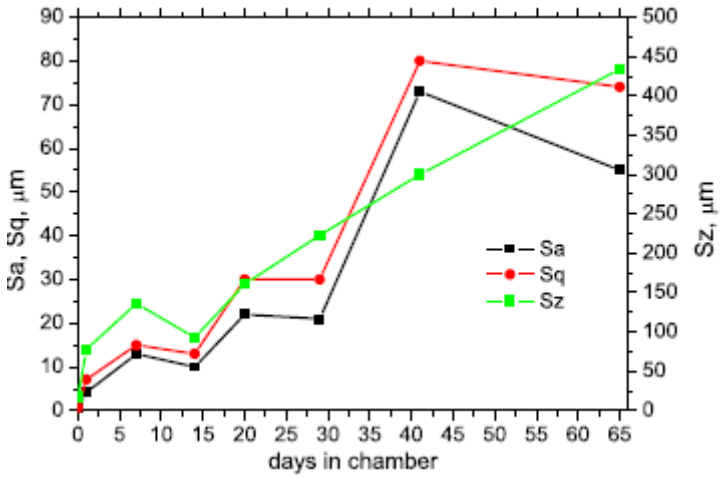

Fig. 3 S parameters as a function of days in chambre

Figure 8 illustrates that MBN in EA and HA progressively decreases with an increase in the exposure time in the chambre. Lower MBN in HA compared with EA results from texture formation during the hot rolling process and the corresponding magnetic reorientation in the rolling direction (EA) [**23**]. For this reason, DWs are preferentially oriented in EA at the expense of HA. It is worth mentioning that all MBN pulses for the bulk state are produced by non-corroded matrix (weak background MBN noise is generated by sensor [**24**]). However, MBN from the corroded surface is composed of the weak pulses originating from the non-corroded spots being embedded in the corroded layer as well as the stronger pulses generated by the underlying non-corroded matrix [**15**]. Fe_3O_4 is referred to a ferromagnetic structure [**1**]; however, motion DWs in Fe_3O_4 cannot be initiated by weak magnetic fields produced by the bipolar sensor (± 4.63 kA m^{-1} for magnetizing conditions listed in **Table 3**). Therefore, the contribution of oxides to the entire MBN is zero. The progressive decrease in MBN in both EA and HA is driven by the superimposing contribution of 4 main aspects. Corroded layer on the surface should be considered as the gap between the pick-up coil, magnetizing poles and ferromagnetic matrix. Growing gap makes weaker magnetic field produced by magnetizing poles in the non-corroded underlying matrix.

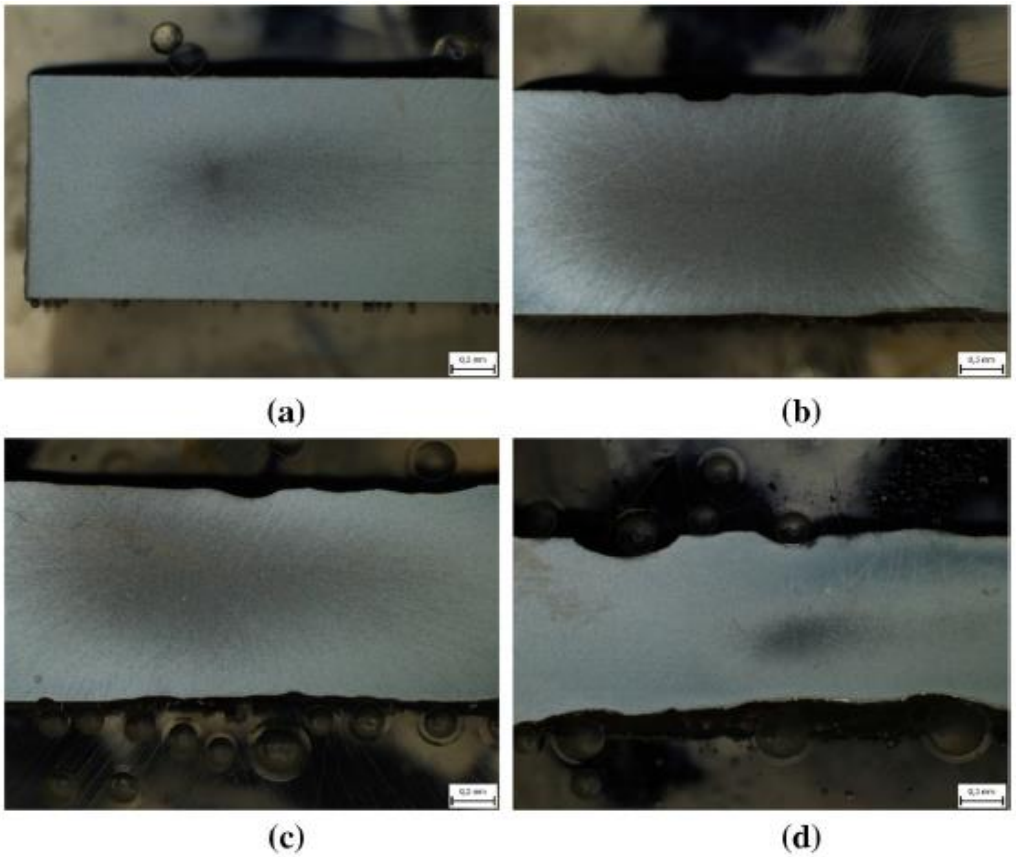

Fig. 4 Cross-sectional views of corroded samples: **a** non-corroded bulk, **b** 14 days in the chamber, **c** 41 days in the chamber, **d** 65 days in the chamber

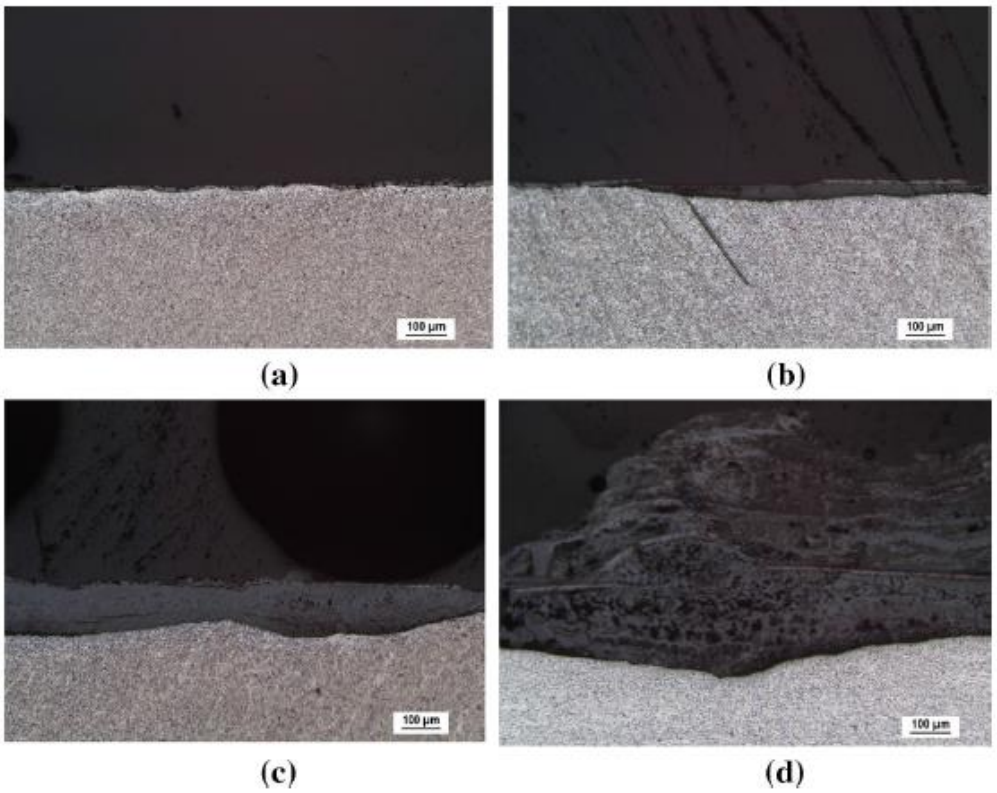

Fig. 5 Metallographic images of corroded samples: **a** 1 day in the chamber, **b** 14 days in the chamber, **c** 41 days in the chamber, **d** 65 days in the chambre

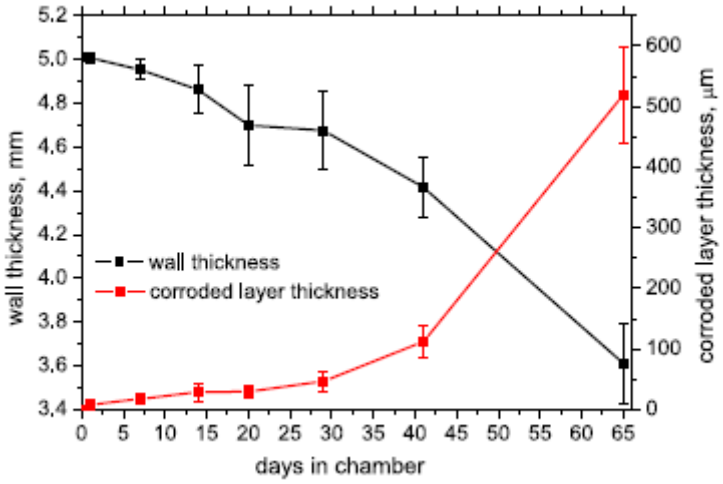

Fig. 6 The thickness of the corroded layer and wall thickness as a function of days in the chambre

This effect decreases the rate of change of magnetic field in timescale as the decisive factor affecting DWs unpinning as well as the rate of magnetization change which is directly linked with MBN [**3, 4**]. Moreover, MBN pulses produced by DWs in motion have to be transmitted to the measuring coil through a corroded layer. Interaction of electromagnetic pulses with oxides (as hard ferromagnetic particles) makes these pulses weaker which in turn decreases detected MBN emission. It is considered that the degree of MBN pulses attenuation grows along with the growing thickness of the corroded layer. The third aspect associated with MBN descent versus corrosion extent is attributed to the height of the surface irregularities, which increases with the time of exposure to the corrosive environment (see **Figs. 2** and **3**). Deng et al. [**25**] reported that the increasing height of surface irregularities attenuates MBN pulses propagating towards the surface; thus this effect makes MBN signal weaker.

Finally, it is worth mentioning that (together with the growing thickness of the corroded layer) also the size of non-corroded fragments in the corroded layer reduces at the expense of their increasing number [**15**].

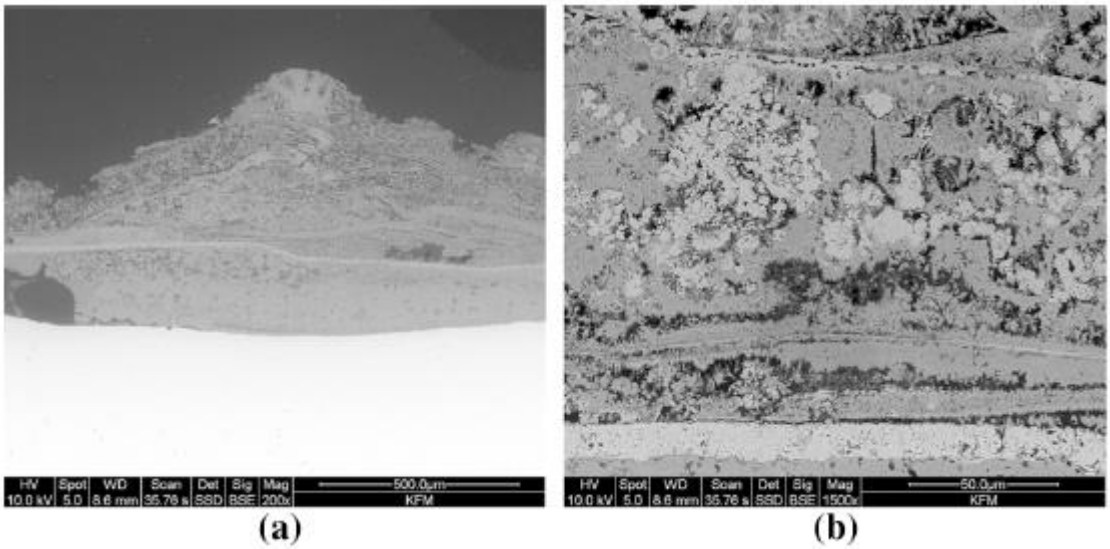

Fig. 7 SEM images of the corroded surface after 65 days in the chamber: **a** large image, **b** detail

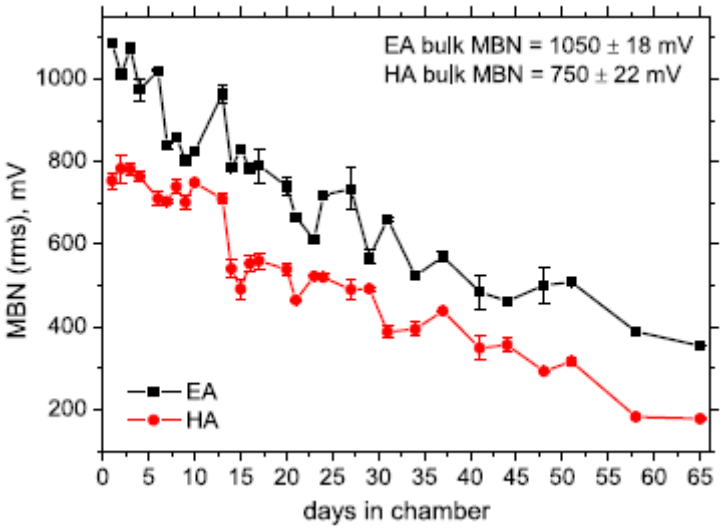

Fig. 8 MBN (rms value) as a function of days in chambre

This effect makes shorter 180° DWs and contributes to the increasing density of 90° DWs [**15**]. Being so, stronger MBN pulses are replaced by weaker ones. The increasing density of 90° DWs is due to the increasing density of boundaries between oxides and non-corroded spots [**26, 27**]. Moreover, it is known that magnetic configuration becomes finer on the free surface or on the boundaries between phases of the different magnetic properties [**1, 28**].

Figure 9 clearly demonstrates the MBN pulses of the highest height (above 2.25 V) are nearly missing for heavily corroded sample (after 65 days in the chamber) as compared with nearly untouched sample (1 day in the chamber). On the other hand, a higher number of weaker pulses can be obtained for the thicker corrosion layers. **Figure 10** shows that the entire number of MBN pulses is growing along with the days in the chamber.

Table 3 Nominal force and true stress in the samples

Nominal force (kN)	Bulk true stress (MPa)	20 days true stress (MPa)	41 days true stress (MPa)	65 days true stress (MPa)
1.875	25	26.6	28.4	34.7
3.75	50	53.2	56.8	69.4
5.625	75	79.8	85.2	104.2
7.5	100	106.4	113.6	138.9
9.375	125	133	142	173.6
11.25	150	159.6	170.5	208.3
13.125	175	186.2	198.9	243
15	200	212.8	227.3	277.8
16.875	225	239.4	255.7	312.5
18.75	250	266	284	347.2
20.625	275	292.5	312.5	381.9
22.5	300	319.2	340.9	416.7

The effective value of the MBN signal is a function of electromagnetic pulses amplitude X_i and their density (number n) as follows:

$$rms = \sqrt{\frac{1}{n}\sum_{i=1}^{n} X_i^2} \qquad (1)$$

The lower MBN for the samples of more developed corrosion extent suggests the subsidiary role of pulses density (in the time scale and the corresponding scale of magnetic field) whereas the influence of MBN pulses height is decisive [**12, 15**]. It should be noticed that the increasing number of MBN pulses (with respect of the increasing corrosion damage) as that shown in **Fig. 10** is driven by:

- the decreasing amplitude of strong MBN pulses as a result of the floating threshold algorithm employed in the Micro Scan software,
- the increasing number of weaker pulses originated from the corroded layer containing the non-corroded regions,
- and attenuation of strong MBN pulses originating from the non-corroder matrix with respect of the increasing thickness of corroded layer.

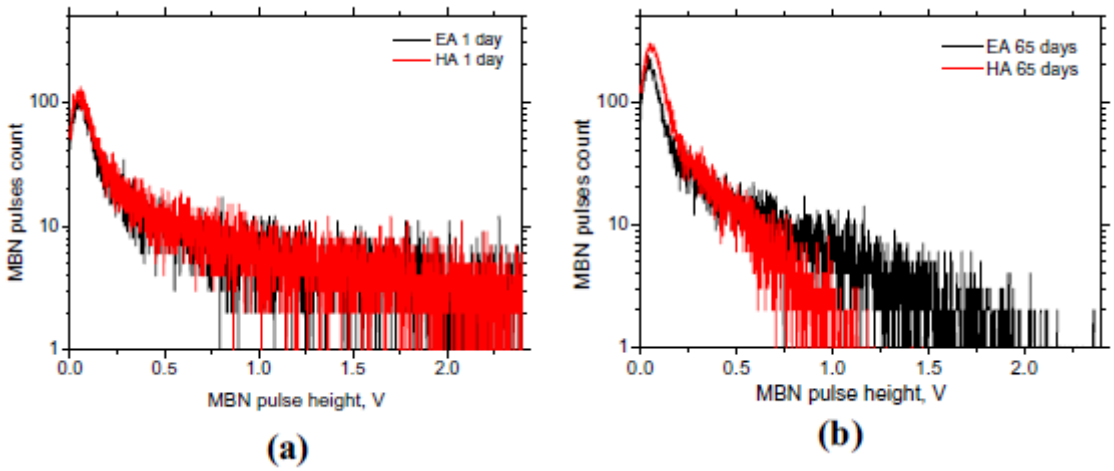

Fig. 9 MBN pulses height distribution: **a** 1 day in chamber, **b** 65 days in chamber

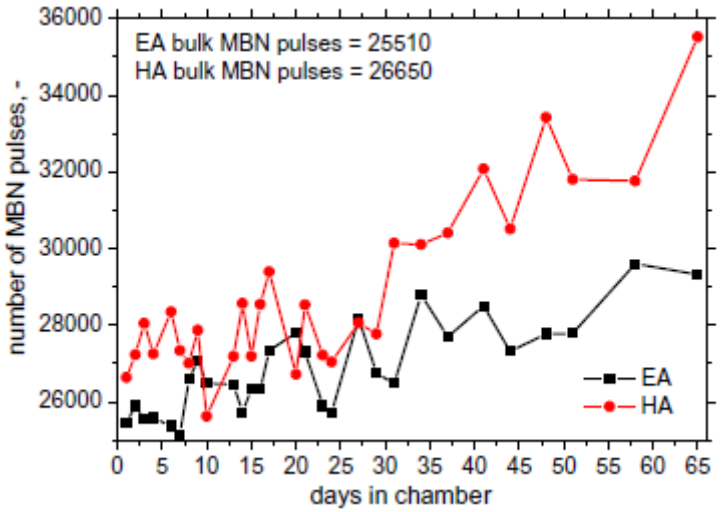

Fig. 10 The number of MBN pulses as a function of days in the chambre

Refinement of DWs structure in the corroded layer and weakening of magnetic field in the non-corroded matrix makes them magnetic harder. **Figures 11** and **12** show that MBN envelopes and the corresponding PP are shifted to the higher magnetic fields along with increasing number of days in the chamber. The maximum of MBN envelopes occur later in magnetic field scale. The higher MBN for the samples of lower corrosion extent is usually attributed to the MBN pulses produced by 180° DWs [**29, 30**]. As soon as the corrosion penetrates deeper, the motion of 180° DWs is limited and takes place at higher magnetic fields. Furthermore, the fraction of MBN pulses generated from 90° DWs motion grows [**29, 30**].

Figures 11 and **12** also depict that the initial higher magnetic hardness (for nearly non-corroded surface) in HA is more as compared with EA which corresponds with the preferential orientation of DWs in EA and higher MBN in this direction.

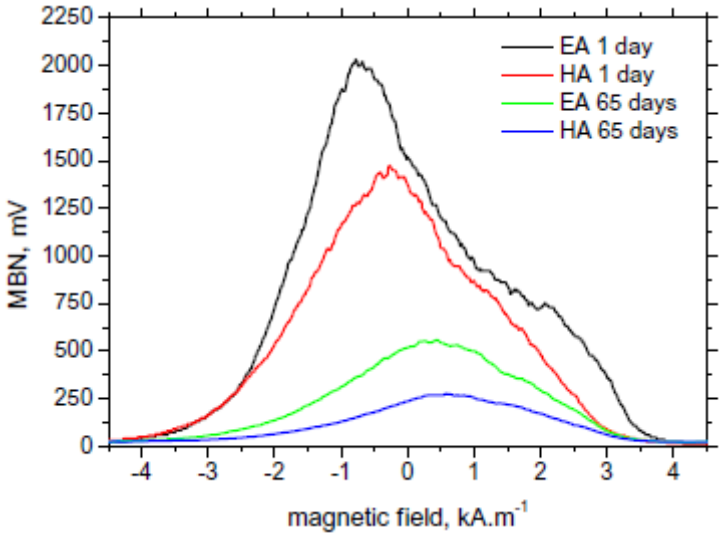

Fig. 11 MBN envelopes

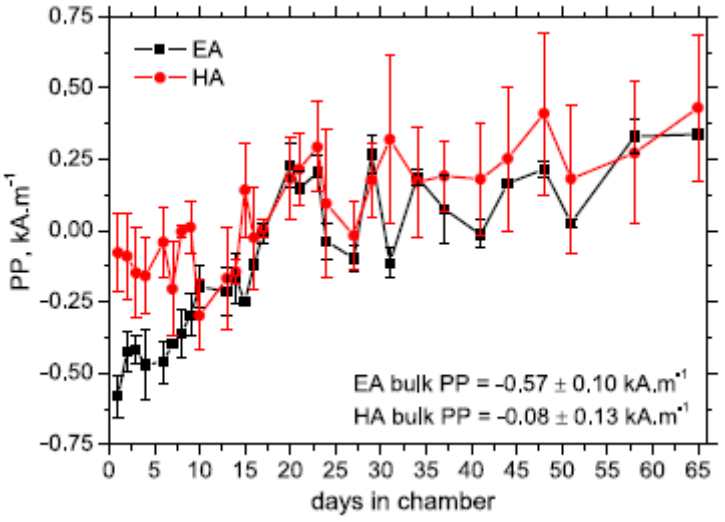

Fig. 12 PP as a function of days in the chambre

However, this anisotropy tends to diminish versus the deeper extent of corrosion. Moreover, as contrasted with MBN and the number of MBN pulses, the evolution of PP versus corrosion extent saturates quite early. A similar evolution (as that reported for PP) can be obtained for the FWHM parameter when the initial growth is followed by moderate descent (see **Fig. 13**).

3.2 Tensile Test

Corrosion extent alters the relation between tensile stress (TS) and MBN. Two fundamental aspects should be discussed. The first one is associated with the corroded layer, which does not transmit exerted load. It is considered that the non-corroded fragments in the corroded layer produce nearly the same MBN signal within the whole range of TS and its contribution to the entire MBN is growing along with the growing corrosion layer thickness only.

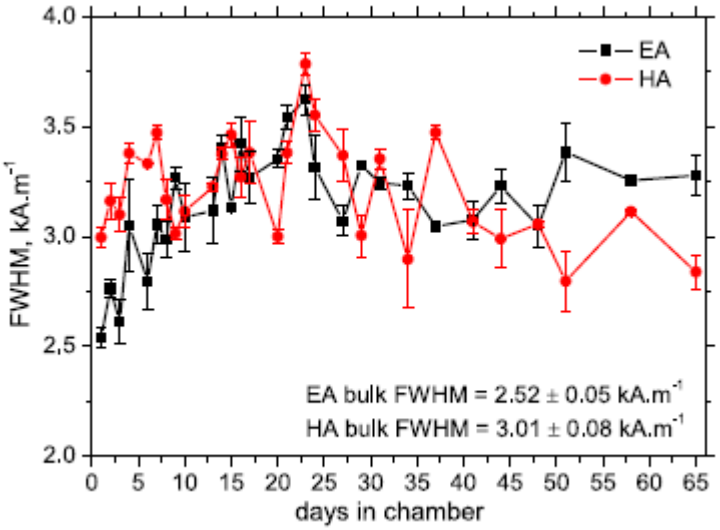

Fig. 13 FWHM as a function of days in the chamber

The second aspect is associated with the reduction of the effective cross-sectional area (see **Fig. 6**).

$$true\ stress = \frac{nominal\ force}{wall\ cross\text{-}sectional\ area} \qquad (2)$$

As mentioned, the samples were loaded by the progressively increasing uniaxial TS from 0 up to 300 MPa with the increment of 25 MPa. The nominal loading force for the untouched (bulk) sample of the wall thickness of 5 mm and the aforementioned sample width 15 mm is listed in **Table 3**. This nominal force (**Table 3**) was kept constant for all samples corroded in the chamber. However, the true stress is different due to the reduced wall thickness and the corresponding effective cross-sectional area. The true TS, as listed in Table 3 for the samples in the chamber for 20, 41 and 65 days, was calculated using Eq. (**2**) with the wall thickness obtained from **Fig. 6**. **Figure 14**a demonstrates that the relation between

TS and MBN is flat for lower TS followed by a moderate decrease in MBN (in the case of the bulk sample). DWs tend to rotate towards the direction of tensile stress which in turn increases the amplitude of MBN impulses [**4, 6**]. However, this effect vanishes when all DWs are fully oriented in the direction of tensile stress and the corresponding energy of magnetocrystalline anisotropy is low [**1, 28, 31**]. Beyond the critical stress MBN drops down versus TS since the magnetoelastic energy predominates. As soon as the corrosion extent is deeper, the relation between TS and MBN is altered. The initial growth of MBN in the region of lower TS is followed by the moderate descent of MBN at higher TS. It should be noticed that the reduced wall thickness for the heavily corroded samples increases gently magnetic flux density. Such behaviour would make MBN emission stronger but it does not. **Figures 8** and **14**a demonstrate that this effect is only minor since MBN exhibits the opposite evolution due to predominating contribution of the corroded layer increasing in thickness. This layer attenuates sample magnetisation as well as generated MBN pulses as it was discussed earlier.

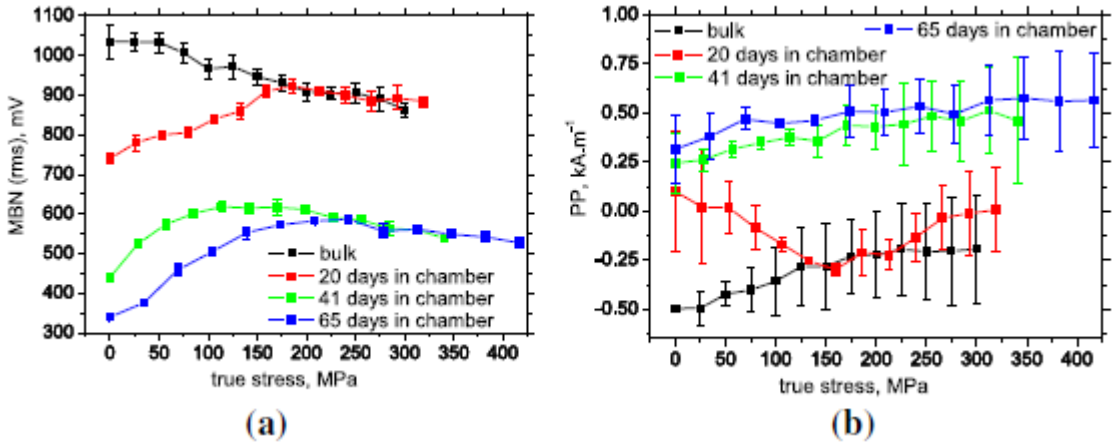

Fig. 14 MBN (rms value) and PP versus tensile stress (EA): **a** MBN (rms), **b** PP

Amiri et al. [**31**] have already demonstrated that the energy of magnetocrystalline anisotropy prevails when MBN grows along with tensile stresses and the reversed evolution is due to the predomination of magnetostriction. However, it should be noticed that in this particular case, the significant role in this evolution takes corroded layer, as the region composed of oxides and non-corroded fragments, which decrease in size at the expense of their increasing number. It seems that the presence of corroded layer and especially small embedded ferromagnetic fragments alters energy of magnetocrystalline anisotropy and/ or magnetostriction energy since the increasing thickness of corrode layer remarkably affects not only MBN (as well as the extracted MBN features) but also the relationship MBN (rms) versus stress state (see **Fig. 14**a). It is considered that the preferential matrix orientation after rolling (for the bulk state) which consumes the energy of magnetocrystalline anisotropy becomes lost when the ferromagnetic fragments in the corroded layer are developed. Fragmentation in the corroded matrix as well as generation of new boundaries between the oxides and the ferromagnetic fragments alters DWs alignment and increases the density of 90° DWs at the expense of 180° DWs. For these reasons, the evolution of MBN along with true stress as that shown in **Fig. 14**a is altered.

The evolution of *PP* versus TS (see **Fig. 14**b) is usually inversely proportional to the relation between MBN and TS [**10, 31**]. Really, **Fig. 14**b illustrates that for the bulk sample and the sample with lower corrosion extent (20 days in the chamber), the descending region of MBN correlates with the growing PP and vice versa. However, in the case of heavily corroded samples, the moderate increase in PP can be reported and is followed by saturation for the highest TS. Increasing rate of magnetization change

usually results into stronger MBN which occurs earlier in the magnetic field and vice versa. Therefore, the higher MBN (rms) is associated with lower PP. This finding is proved in **Fig. 14**b for the bulk sample as well as the sample being 20 days in the chamber. However, it seems that this evolution becomes lost when the contribution of non-corroded fragments in the corroded layer prevails with respect of reading depth of MBN (see also **Fig. 6**). As soon as the thickness of corroded layer dominates in the estimated reading depth of MBN, PP progressively grows with the trues stress (see the evolutions of PP for the sample being corroded 40 and 65 days in the chamber).

FWHM exhibits quite good sensitivity for the assessment of TS (see **Fig. 15**a). FWHM of MBN envelopes exhibits quite good sensitivity with respect to TS [**32**]. **Figure 15**a demonstrates that FWHM exhibits progressively decreases along with TS but the FWHM-TS curves are mixed in the region of lower TS without clear tendency with respect to the variable thickness of the corroded layer. The number of MBN pulses for corroded samples drops down in the region of low TS (as compared with the bulk sample) followed by early saturation (see **Fig. 15**b).

4 Conclusions

Main findings of this study can be summarized as follows:

- effective value of MBN emission progressively decreases along with the increasing extent of corrosion damage whereas the number of all MBN pulses progressively grows,
- PP and FWHM of MBN envelopes exhibit the initial growth along with the increasing extent of corrosion damage followed by the early saturation,
- superimposing contribution of corroded layer makes assessment of stress via MBN technique more difficult,
- corroded samples exhibit the initial growth of MBN (effective value) at the lower TS followed by the decreasing region at the higher ones,
- evolution of PP versus TS is reversed as compared with evolution of the effective value when the thickness of corroded layer lower,
- as soon as the thickness of corroded layer dominates in the MBN reading depth, PP grows progressively with TS,
- FWHM decreases along with increasing thickness of corroded layer as well as the superimposing TS,
- number of MBN pulses initially drops down with the stress followed by early saturation for higher TS.

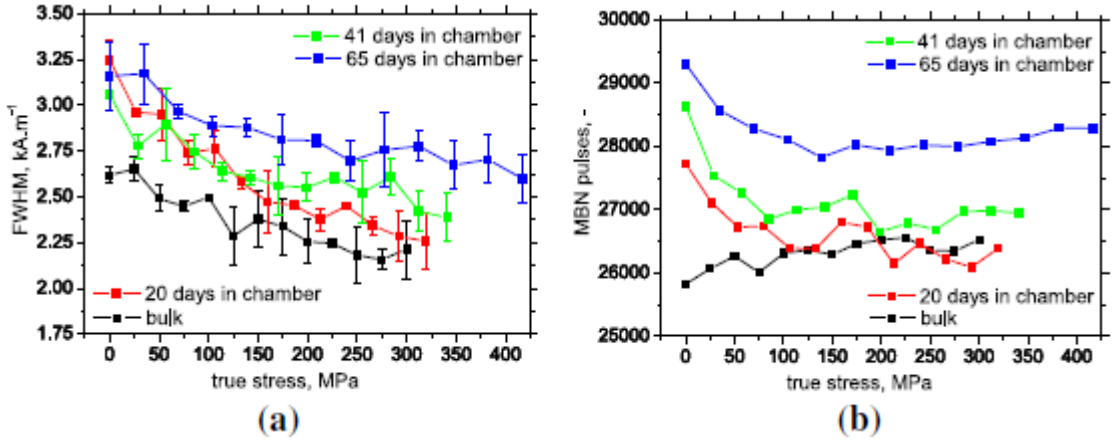

Fig. 15 FWHM and number of MBN pulses versus tensile stress (EA): **a** FWHM, **b** number of MBN pulses

MBN, PP, FWHM and number of MBN pulses versus TS in HA direction do not provide any valuable evolution that could be potentially employed to assess TS when the superimposing influence of variable corrosion extent is considered. The main reason can be viewed in the direction of TS, which is perpendicular against HA and tend to align DWs in EA at the expense of HA.

Finally, it can be concluded that the presence of corroded layer on the surface of S460MC steel makes it difficult to assess the real magnitude of TS when the thickness of the corroded layer varies. Figures 14 and 15 clearly illustrate that none of the analysed MBN parameters exhibits exclusive values with respect of TS and the superimposing corrosion extent. For this reason, it is proposed to assess TS and the thickness of corroded layer by the use of MBN parameters combination.

References

1. Jiles, D.: Introduction to Magnetism and Magnetic Materials, 3rd edn. Taylor & Francis Group, New York (2016)

2. Chikazumi, S.: Physics of Ferromagnetism, 2nd edn. Oxford University Press, Oxford (2005)

3. Varga, R.: Domain Walls and Their Dynamics, 1st edn. Pavol Jozef Šafárik University, Košice (2014)

4. Liu, J., Tian, G.Y., Gao, B., Zeng, K., Zheng, Y., Chen, J.: Micromacro characteristics between domain wall motion and magnetic Barkhausen noise under tensile stress. J. Magn. Magn. Mater. **493**, e165719 (2020). **https://doi.org/10.1016/j.jmmm.2019.165719**

5. Avila, J.A., Conde, F.F., Pinto, H.C., Rodriguez, J., Grijalba, F.A.F.: Microstructural and residuals stress analysis of friction stir welding of X80 pipeline steel plates using magnetic Barkhausen noise. J. Non-Destruct. Eval. **38**, 86 (2019). **https://doi.org/10. 1007/s 10921-019-0625-2**

6. Karpuschewski, B., Bleicher, O., Beutner, M.: Surface integrity inspection on gears using Barkhausen noise analysis. Proc. Eng. **19**, 162-171 (2011). **https://doi.org/10.1016/j.proeng.2011.11.096**

7. Sorsa, A., Santa-Aho, S., Wartiainen, J., Souminen, L., Vippola, M., Leviska, K.: Effect of shot peening parameters to residual stress profiles and Barkhausen noise. J. Non-Destruct. Eval. **37**, 1-11 (2018). **https://doi.org/10.1007/s10921-018-0463-7**

8. Gatelier-Rothea, C., Chicois, J., Fougeres, R., Fleischmann, P.: Characterization of pure iron and (130 p.p.m.) carbon-iron binary alloy by Barkhausen noise measurements: study of the influence of stress and microstructure. Acta Metal. **46**, 4873-4882 (1998). **https://doi.org/10.1016/S 1359-6454(98)00205-5**

9. Neslušan, M., Čížek, J., Kolařík, K., Minárik, P., Čilliková, M., Melikhová, O.: Monitoring of grinding burn via Barkhausen noise emission in case-hardened steel in large-bearing production. J. Mater. Process. Technol. **240**, 104-117 (2017). **https://doi.org/ 10.1016/j.matprotec.2016.09.015**

10. Čížek, J., Neslušan, M., Čilliková, M., Mičietová, A., Melikhova, O.: Modification of steel surfaces induced by turning: nondestructive characterization using Barkhausen noise and

positron annihilation. J. Phys. D Appl. Phys. **47**, 1-17 (2014). **https://doi. org/10.108 8/0022-3727/47/44/445301**

11. Stupakov, A., Perevertov, O., Tomáš, I., Skrbek, B.: Evaluation of surface decarburization depth by magnetic Barkhausen noise technique. J. Magn. Magn. Mater. **323**, 1692-1697 (2011). **https:// doi.org/10.1016/j.jmmm.2011.01.039**

12. Neslušan, M., Minárik, P., Grenčík, J., Trojan, K., Zgútová, K.: Non-destructive evaluation of the railway wheel surface damage after long-term operation via Barkhausen noise technique. Wear **420-421**, 195-206 (2019). https://doi.org/10.1016Zj.wear.2018. 10.0146

13. Zgútová, K., Neslušan, M., Kolářik, K., Šrámek, J.: Non-destructive Evaluation of Stress State of the Highway Bridge via Barkhausen Noise Technique, Progress in Mechanics and Materials in Design. In: 7th International conference on Mechanics and Materials in Design, Albufeira, Portugal (2017)

14. Neslušan, M., Bahleda, F., Trojan, K., Pitoňák, M., Zgútová, K.: Monitoring of over-stressing of steel wires by the Barkhausen noise. J. Magn. Magn. Mater. **513**, e167134 (2020). **https://doi. org/10.1016/j.jmmm.2020.167134**

15. Neslušan, M., Bahleda, F., Minárik, P., Zgútová, K., Jambor, M.: Non-destructive monitoring of corrosion extent in steel rope wires via Barkhausen noise emission. J. Magn. Magn. Mater. **484**, 179-187 (2019). **https://doi.org/10.1016/j.jmmm.2019.04.017**

16. Neslušan, M., Bahleda, F., Moravčík, M., Zgútová, K., Pastorek, F.: Assessment of tendons prestressing after long-term service via the Barkhausen noise technique. Materials **12**, e3450 (2019). **https://doi.org/10.3390/ma12203450**

17. Anania, L., Badala, A., D'Agata, G.: Damage and collapse mode of existing post tensioned precast concrete bridge: the case of Petrulla viaduct. Eng. Struct. **162**, 226-244 (2018). **https://doi. org/10.1016/j.engstruct.2018.02.039**

18. Zergoug, M., Kamel, G., Benchaala, A.: Determination of Micro Structural Corrosion by BN, Research Report of Laboratoire d'Electronique et d'Electrotechnique, Alger (2004)

19. Alamin, M., Tian, G.Y., Andrews, A., Jackson, P.: Principal component analysis of pulsed eddy current response from corrosion in mild steel. IEEE Sens. J. **12**, 2548-2553 (2012). **https://doi.org/ 10.1109/JSEN.2012.2195308**

20. Xu, J., Sun, H., Cai, S.: Effect of symmetrical broken wires damage on mechanical characteristics of stay cable. J. Sound Vib. **461**, e114920 (2019). **https://doi.org/10.1016/j.jsv.2019.114920**

21. Li, S., Hu, P., Zhao, X., Chen, K., Li, J.: Atmospheric corrosion performance of wire rope sling in sulphur dioxide-polluted environment. Adv. Mech. Eng. **9**, 1-12 (2017). **https://doi.org/10. 1177/1687814017707479**

22. Antunes, R.A., Ichikawa, R.U., Martinez, L.G., Costa, I.: Characterization of corrosion products on carbon steel exposed to natural weathering and to accelerated corrosion tests. Int. J. Corros. (2014). **https://doi.org/10.1155/2014/419570**

23. Manh, T.L., Caleyo, F., Hallen, J.M., Pérez-Benitez, J.A., Espina-Hernández, J.H.: Novel method for the accurate determination of magnetocrystalline energy from Barkhausen noise in ferromagnetic materials. Mater. Sci. Eng. B **225**, 98-107 (2017). **https:// doi.org/10.1016/j.mseb.2017.08.015**

24. Blažek, D., Neslušan, M., Mičica, M., Pištora, J.: Extraction of Barkhausen noise from the measured raw signal in high-frequency regimes. Measurement **94**, 456-463 (2016). **https://doi.org/10. 1016/j.measurement.2016.08.022**

25. Deng, Y., Li, Z., Chen, J., Qi, X.: The effect of the structure characteristics on Magnetic Barkhausen noise in commercial steels. J. Magn. Magn. Mater. **451**, 276-282 (2018). **https://doi.org/10. 1016/j.jmmm.2017.11.041**

26. Puppin, E.: Statistical properties of Barkhausen noise in thin Fe films. Phys. Rev. Lett. **84**, e5415 (2000). **https://doi.org/10.1103/ PhysRevLett.84.4705**

27. Hubert, A., Schafer, R.: Magnetic Domains: The Analysis of Magnetic Microstructures, 1st edn. Springer, Berlin (1998)

28. Cullity, B.D., Graham, C.D.: Introduction to the Magnetic Materials, 2nd edn. IEEE Press, New Jersey (2009)

29. Martínez-Ortiz, P., Pérez-Benitez, J.A., Espina-Hernández, J.H., Caleyo, F., Hallen, J.M.: On the estimation of the magnetic easy axis in pipeline steels using magnetic Barkhausen noise. J. Magn. Magn. Mater. **374**, 67-74 (2015). **https://doi.org/10.1016/j.jmmm. 2015.10.036**

30. Chávez-Gonzalez, A.F., Martínez-Ortiz, P., Pérez-Benitez, J.A., Espina-Hernández, J.H., Caleyo, F.: Comparison of angular dependence of magnetic Barkhausen noise of hysteresis and initial magnetization curve in API5L steel. J. Magn. Magn. Mater. **446**, 18-27 (2017). **https://doi.org/10.1016/j.jmmm.2017.08.089**

31. Amiri, M.S., Thielen, M., Rabung, M., Marx, M., Szielasko, K. , Boller, Ch.: On the role of crystal and stress anisotropy in magnetic Barkhausen noise. J. Magn. Magn. Mater. **372**, 16-22 (2014). **https://doi.org/10.1016/j.jmmm.2014.07.038**

32. Šrámek, J., Neslušan, M., Bahleda, F., Zgútová, K., Schenk, P.: Influence of sample size and magnetizing voltage on Barkhausen noise during bending and uniaxial tensile test. Acta Phys. Polonica A **137**, 640-643 (2020). **https://doi.org/10.12693/APhysPolA.137.640**